Geomicrobiology Journal

ISSN: 0149-0451 (Print) 1521-0529 (Online) Journal homepage: http://www.tandfonline.com/loi/ugmb20

Interactions Between Fe(III)-oxides and Fe(III)-phyllosilicates During Microbial Reduction 2: Natural Subsurface Sediments

T. Wu, A. M. Griffin, C. A. Gorski, E. S. Shelobolina, H. Xu, R. K. Kukkadapu & E. E. Roden

To cite this article: T. Wu, A. M. Griffin, C. A. Gorski, E. S. Shelobolina, H. Xu, R. K. Kukkadapu & E. E. Roden (2017) Interactions Between Fe(III)-oxides and Fe(III)-phyllosilicates During Microbial Reduction 2: Natural Subsurface Sediments, Geomicrobiology Journal, 34:3, 231-241, DOI: 10.1080/01490451.2016.1174758

To link to this article: http://dx.doi.org/10.1080/01490451.2016.1174758

Accepted author version posted online: 19 Apr 2016.
Published online: 19 Apr 2016.

GEOMICROBIOLOGY JOURNAL
2017, VOL. 34, NO. 3, 231–241
http://dx.doi.org/10.1080/01490451.2016.1174758

Taylor & Francis
Taylor & Francis Group

Interactions Between Fe(III)-oxides and Fe(III)-phyllosilicates During Microbial Reduction 2: Natural Subsurface Sediments

T. Wu[a], A. M. Griffin[b], C. A. Gorski[b], E. S. Shelobolina[a], H. Xu[a], R. K. Kukkadapu[c], and E. E. Roden[a]

[a]Department of Geoscience, University of Wisconsin-Madison, Madison, Wisconsin, USA; [b]Department of Civil and Environmental Engineering, Pennsylvania State University, University Park, Pennsylvannia, USA; [c]Environmental Molecular Sciences Laboratory, Pacific Northwest National Laboratory, Richland, Washington, USA

ABSTRACT

Dissimilatory microbial reduction of solid-phase Fe(III)-oxides and Fe(III)-bearing phyllosilicates (Fe(III)-phyllosilicates) is an important process in anoxic soils, sediments and subsurface materials. Although various studies have documented the relative extent of microbial reduction of single-phase Fe(III)-oxides and Fe(III)-phyllosilicates, detailed information is not available on interaction between these two processes in situations where both phases are available for microbial reduction. The goal of this research was to use the model dissimilatory iron-reducing bacterium (DIRB) *Geobacter sulfurreducens* to study Fe(III)-oxide vs. Fe(III)-phyllosilicate reduction in a range of subsurface materials and Fe(III)-oxide stripped versions of the materials. Low-temperature (12 K) Mossbauer spectroscopy was used to infer changes in the relative abundances of Fe(III)-oxide, Fe(III)-phyllosilicate, and phyllosilicate-associated Fe(II) (Fe(II) phyllosilicate). A Fe partitioning model was employed to analyze the fate of Fe(II) and assess the potential for abiotic Fe(II)-catalyzed reduction of Fe(III)-phyllosilicates. The results showed that in most cases Fe(III)-oxide utilization dominated (70–100%) bulk Fe(III) reduction activity, and that electron transfer from oxide-derived Fe(II) played only a minor role (ca. 10–20%) in Fe partitioning. In addition, the extent of Fe(III)-oxide reduction was positively correlated to surface area-normalized cation exchange capacity and the Fe(III)-phyllosilicate/total Fe(III) ratio. This finding suggests that the phyllosilicates in the natural sediments promoted Fe(III)-oxide reduction by binding of oxide-derived Fe(II), thereby enhancing Fe(III)-oxide reduction by reducing or delaying the inhibitory effect that Fe(II) accumulation on oxide and DIRB cell surfaces has on Fe(III)-oxide reduction. In general our results suggest that although Fe(III)-oxide reduction is likely to dominate bulk Fe(III) reduction in most subsurface sediments, Fe(II) binding by phyllosilicates is likely to play a key role in controlling the long-term kinetics of Fe(III) oxide reduction

ARTICLE HISTORY
Received November 2015
Accepted March 2016

KEYWORDS
Iron reduction; subsurface microbiology; sediments; iron oxides; phyllosilicates

Introduction

Microbial reduction of solid-phase Fe(III)-oxides and Fe (III)-bearing phyllosilicates (Fe(III)-phyllosilicates) is an important process in anoxic soils, sediments and subsurface materials (Dong et al. 2009; Lovley 1993; Roden and Zachara 1996; Stucki and Kostka 2006). Dissimilatory iron-reducing bacteria (DIRB) are capable of oxidizing organic matter and hydrogen with reduction of both Fe(III)-oxides and Fe(III)-bearing phyllosilicates as an electron acceptor. Microbial reduction of Fe(III)-oxides and associated biomineralization processes have been well studied in pure, single-phase Fe(III) oxide systems under controlled conditions (Fredrickson et al. 1998, 2003; Kukkadapu et al. 2004; Roden and Zachara 1996; Zachara et al. 1998, 2002), and the main factors that control the rate and extent of microbial Fe(III) oxide reduction have been extensively interpreted (Roden 2008).

The potential for microbial reduction of Fe(III)-phyllosilicates has also received significant attention. Several single-phase model Fe(III)-phyllosilicates have been studied, e.g., nontronites NAu-1 and NAu-2, and ferruginous smectite SWa-1 (Dong et al. 2009; Jaisi et al. 2005, 2007a; Pentrakova et al. 2013; Stucki and Kostka 2006). These model phyllosilicates have relatively high Fe(III) content and a relatively high extent of microbial reduction by DIRB. The rate and extent of microbial reduction of Fe(III)-phyllosilicates are primarily controlled by the properties of phyllosilicates themselves. In particular, the site of Fe(III) in the phyllosilicate structure (e.g., tetrahedral vs. octahedral) can affect its susceptibility to microbial reduction (Jaisi et al. 2005). Furthermore, mineralogical factors (e.g., the proportion of smectite in illite–smectite mixed interlayer minerals) also strongly influence microbial reduction of model phyllosilicates (Bishop et al. 2011; Liu et al. 2012; Zhang et al. 2012). Recent studies have demonstrated that phyllosilicate thermodynamic properties ultimately set an upper limit on the long-term extent of microbial Fe(III) phyllosilicate reduction (Luan et al. 2014, 2015a, 2015b).

There are important differences between phyllosilicate minerals found in soils and sediments compared to model minerals in relatively pure deposits. Phyllosilicate minerals from soils and sediments often have interlayered structures, a mixed order of stacking (e.g., Sawhney 1989), and are impure (e.g., there are multiple phyllosilicate minerals, and other Fe-containing impurities such as Fe

CONTACT E. E. Roden eroden@geology.wisc.edu Department of Geoscience, University of Wisconsin, Madison, WI 53706, USA.

(III)-oxides). The interaction between Fe(III)-oxides and Fe(III)-phyllosilicates may play an important role in microbial clay reduction in soils or sediments (Wu et al. 2012, 2015). Although various studies have documented the relative extent of microbial Fe(III) oxide and Fe(III) phyllosilicate reduction in sediments (Akob et al. 2008; Dong et al. 2003; Kukkadapu et al. 2006; Mohanty et al. 2008; Wu et al. 2012), information on potential impact of natural sediment mineralogy and Fe phases on bulk microbial Fe(III) mineral reduction is still limited.

In this study, the model DIRB *Geobacter sulfurreducens* was used to study microbial Fe(III) oxide and Fe(III) phyllosilicate reduction of a range of subsurface materials, with the explicit goal of determining the relative contribution of Fe(III) phyllosilicate vs. Fe(III) oxide to bulk Fe(III) reduction. Also of interest was (1) the rate and extent of Fe(III) phyllosilicate reduction in pristine materials compared to Fe(III)-phyllosilicates in Fe(III) oxide stripped sediments recovered by a previously developed citrate-bicarbonate-dithionite (CDB) extraction and reoxidation procedure (Wu et al. 2012); and (2) controls on the extent of Fe(III) oxide reduction in relation to the fate of Fe(II) generated during oxide reduction. This study represents a companion to Wu et al. (2015) which examined microbial reduction of Fe(III) oxide stripped subsurface sediment coated with varying quantities of synthetic goethite. In agreement with observations with synthetic goethite-coated sediments (Wu et al. 2015), the results reported here suggest that in most cases Fe(III) oxide utilization is likely to dominate bulk Fe(III) reduction activity, and that electron transfer from oxide-derived Fe(II) to Fe(III)-phyllosilicates plays only a minor role in Fe partitioning. However, our results suggest that phyllosilicates may play a key role in controlling the long-term extent of Fe(III) oxide reduction by binding oxide-derived Fe(II), thereby reducing or delaying the negative impact of Fe(II) sorption to oxide and DIRB cell surfaces on oxide reduction.

Materials and methods

Subsurface sediments

Six U.S. Department of Energy (DOE)-relevant subsurface materials were used for this study, including: (1) Pliocene and Pleistocene Age Atlantic coastal plain sediments (designated Oyster sediment) collected from sediment cores on the Delmarva Peninsula, Virginia, USA, which consists of quartz sand plus a mixture of Si- and Al-rich nanophases of variable crystallinity with interspersed smectite and agglomerates of goethite nanoparticles (Penn et al. 2001; Zachara et al. 1995); (2) three weathered saprolites (designated field research center [FRC], SCR1 and SCR4) from the Area 2 site at the U.S. DOE's FRC at Oak Ridge National Laboratory in Tennessee, which consist mainly of clays (smectite, illite and kaolinite) heavily coated with mainly crystalline Fe(III)-oxides (Barnett et al. 2000; Moon et al. 2006); and (3) sediments from the grounds of a former uranium ore processing facility in Rifle, Co (designated Rifle sediment). This site, designated the Old Rifle site, is part of the Uranium Mill Tailings Remedial Action program of the U.S. DOE (Anderson et al. 2003). Sediments at the site consist of quartz sand and a mixture of clays (montmorillonite, muscovite and clinochlore) and crystalline Fe(III)-oxides. Lastly, (4) Pliocene-age fine-grained sediment from the upper Ringold Formation (designated Ringold sediment) at the Hanford 300 Area Site in Eastern WA, which consists mainly of a mixture of clays (smectite, muscovite, vermiculite and chlorite) with relatively small amounts of crystalline Fe(III)-oxides (Lee et al. 2012).

Wet chemical extractions

All of the materials were wet sieved (<45 μm) and freeze dried before wet chemical treatment. Citrate–dithionite–bicarbonate (CDB) extraction at 80°C (CDB-80C), which reductively dissolves both amorphous and crystalline Fe(III)-oxides (Mehra and Jackson 1960), was used to remove Fe(III)-oxides, after which the materials were reoxidized by treatment with 3% H_2O_2. Details of the extraction and reoxidation procedures are given in Wu et al. (2012). The reoxidized solids were washed twice with 10% 1,4-Piperazinediethanesulfonic acid (PIPES) buffer, followed by two washes with deionized water. The washed solids were then freeze dried. Prior studies with the "FRC" material employed in this study (Wu et al. 2012) showed that the CDB extraction and reoxidation procedure did not alter phyllosilicate mineralogy (d-spacing) and that Fe redox speciation in the reoxidized material was similar to that in the pristine sediment.

The total Fe and Fe(II) contents of the pristine and CDB-extracted materials were determined by the HF-1,10-phenanthroline (HF-phenanthroline) method, which recovers Fe from both iron oxides and phyllosilicates. The HF-phenanthroline method used was a modification of the method described by Komadel and Stucki (1988), in which hydroxylamine sulfate (rather than light) was used to reduce all Fe in the extract for determination of total Fe (Amonette and Templeton 1998).

The freeze-dried materials were used for cation exchange capacity (CEC) and BET surface area measurements. CEC was measured by using the ammonium acetate (pH 7) method (Sumner and Miller 1996). The specific surface area of the pristine materials was determined by multipoint BET analysis (Micromeritics Model Gemini).

Microbial reduction experiments

The six pairs of CDB-extracted/reoxidized and pristine sediments were employed in microbial reduction experiments with the model DIRB, *G. sulfurreducens* (Caccavo et al. 1994; Methe et al. 2003). All experiments were conducted with washed, acetate/fumarate-grown cells in a PIPES (10 mM) buffered (pH 6.8) growth medium containing (g/l) NH_4Cl (0.25), $NaH_2PO_4{\cdot}H_2O$ (0.07), and KCl (0.1) (Lovley and Phillips 1988). Acetate (20 mM) served as the electron donor, and Fe(III) in sediments as the only electron acceptor. All cultures contained 50 g/l of sediment, which (by virtue of the differing Fe(III) contents of the materials) led to bulk Fe(III) concentrations ranging from 7 to 52 mmol/l. Fe(III) reduction was monitored by measuring the accumulation of HF-phenanthroline extractable Fe(II). Aqueous samples were acidified in 0.5 M HCl and the aqueous Fe was measured by ICP-OES.

XRD and Mossbauer analysis

Oriented aggregate mounts of all seven sediments were prepared to identify phyllosilicates and other minerals by X-ray diffraction (XRD). Sediments were mixed with a small amount of distilled water and sonicated for 1 h. The suspension was gently transferred to a petrographic slide, and air-dried slowly. The (101) peak of quartz in all the XRD patterns was used as an internal calibrator. The samples were analyzed with a Scintag PADV X-ray Diffractometer (Cu Kα radiation). The Scintag diffractometer was operated at 45 kV, 40 mA and used a 2-mm divergence slit, 4-mm incident scatter slit, 1-mm diffracted beam scatter slit, and 0.5-mm receiving slit. A step size of 0.02° and a dwelling time of 2 sec per step were used for collecting all the step-scan diffraction patterns.

Mossbauer analysis of unreduced natural sediments was performed on air-dried samples, whereas analysis of biologically reduced sediments was performed on samples dried under a stream of O_2-free N_2. Only spectra obtained at 12 K, where Fe (III)-oxides and certain Fe(II) phases (e.g., siderite) magnetically order, are reported in this study. All samples (reduced and unreduced) were analyzed at Pennsylvania State University using a SVT400 cryogenic Mossbauer system (SEE Co., USA). The ^{57}Co radioactive source (~50 m Ci) was in a Rh matrix at room temperature. All hyperfine parameters are reported relative to α-Fe foil at room temperature. Samples were sealed between two pieces of 5 ml kapton tape inside an anaerobic chamber to avoid oxidation when transferring the sample from the anaerobic chamber to the sample holder.

Spectral fitting of Mossbauer spectra was done using the Recoil Software (University of Ottawa, Ottawa, Canada). All fits were done using a Voigt-based model (Rancourt and Ping 1991). For simplicity, only three Fe pools were considered for the fitting: (1) a sextet representing Fe(III) oxide (i.e., goethite), (2) a doublet representing Fe(III) phyllosilicate and (3) a doublet representing Fe(II) phyllosilicate. As explained in Wu et al. (2015), although the data could be fit to a more complex model that included multiple Fe(III) oxide pools, the improvement in overall fit was minimal and in some cases use of a more complex model led to inconsistencies in Mossbauer-derived estimates of Fe(III) oxide reduction. Hence the approach adopted for analysis of microbially reduced synthetic goethite-coated subsurface sediment (Wu et al. 2015) was retained in this study of natural Fe(III) oxide bearing materials.

The Lorentzian linewidth was held at 0.14 mm/sec during fitting, as it was the linewidth measured on the spectrometer for an ideally thick α-Fe foil. For all fits, unless otherwise noted, the chemical shift (CS), quadrupole splitting (QS), hyperfine parameter (H), and relative areas between sites were allowed to float during fitting. In some cases, two hyperfine field components were used to model the Fe(III) oxide sextets to account for interline broadening. For each sample analyzed, the relative abundance of Fe(III) oxide, Fe(III) phyllosilicate, and Fe(II) phyllosilicate was determined by multiplying the fractional phase area by the total HF-phenanthroline extractable Fe content. Error terms for the Mossbauer-derived Fe pool size estimates (and changes in them) were determined by propagation of uncertainties (Bevington and Robinson 1992) in model fits to Mossbauer spectra.

Results

Iron content and phyllosilicate mineralogy

The relative abundance of Fe(II) in CDB-extracted and reoxidized sediments was comparable to that of pristine sediments (Table 1). As previously discussed (Wu et al. 2012), this result implies that most of the Fe(II) in the pristine sediment was present in the structure of Fe-bearing phyllosilicates. The remaining Fe was present as Fe(III)-oxides that resisted CDB extraction in SCR4, Rifle and Ringold materials. The results of prior studies have shown that the residual Fe(III)-oxides were not reduced by *G. sulfurreducens* (Wu et al. 2012, 2015). More Fe was present as Fe(III)-oxides than as Fe(III)-phyllosilicates for all but the Ringold sediment, in which Fe(III)-oxides accounted for only ca. 10% of total Fe.

Phyllosilicates mineralogy varied significantly among the different sediments. Smectite, illite and kaolinite were identified (by XRD) in all materials (Figure 1). Smectite was the dominant

Table 1. Fe content of pristine sediments and CDB-stripped sediments.

Materials (<45 μm)	BET SA[a] ($m^2\ g^{-1}$)	Fe(II)[b] (μ mol g^{-1})	Total Fe[b] (μ mol g^{-1})	Total Fe(III)[c] (μ mol g^{-1})	Fe(II) phyllo[d] (μ mol g^{-1})	Fe(III) phyllo[d] (μ mol g^{-1})	Fe(III) oxide[d] (μ mol g^{-1})
FRC	14.4	17.6 ± 0.5	421.8 ± 26.4	404.2 ± 26.4	36.7 ± 5.9	89.0 ± 6.8	296.1 ± 19.3
SCR1	13.6	20.6 ± 1.3	418.9 ± 25.2	398.3 ± 25.2	23.6 ± 4.2	102.3 ± 7.1	293.2 ± 18.2
SCR4	32.1	87.2 ± 6.3	850.2 ± 48.1	763.0 ± 48.5	123.11 ± 7.3	292.81 ± 16.7	434.3 ± 24.7
Rifle	17.4	130.7 ± 5.4	586.8 ± 28.8	456.1 ± 29.3	121.29 ± 6.7	184.1 ± 9.8	281.7 ± 16.6
Oyster	38.4	47.8 ± 0.7	716.9 ± 42.5	669.1 ± 42.5	52.4 ± 4.7	144.74 ± 9.1	519.8 ± 31.1
Ringold	25.0	76.3 ± 0.7	552.9 ± 27.1	476.6 ± 27.1	92.39 ± 4.9	407.8 ± 20.2	52.7 ± 3.6
Extracted FRC[e]		12.0 ± 0.1	145.1 ± 10.6	133.1 ± 10.6	48.0 ± 7.2	97.1 ± 9.4	0.00 ± 0.0
Extracted SCR1[e]		20.3 ± 2.9	147.1 ± 6.1	126.8 ± 6.8	41.8 ± 2.9	105.3 ± 5.4	0.00 ± 0.0
Extracted SCR4[e]		121.3 ± 10.9	589.9 ± 17.4	458.1 ± 18.9	116.2 ± 7.3	298.1 ± 13.6	184.64 ± 13.5
Extracted Rifle[e]		154.3 ± 6.1	424.6 ± 19.8	270.3 ± 20.7	136.7 ± 10.6	164.7 ± 13.4	123.13 ± 14.0
Extracted Oyster[e]		56.6 ± 1.3	250.8 ± 12.6	194.2 ± 12.6	91.0 ± 7.2	159.8 ± 9.7	0.00 ± 0.0
Extracted Ringold[e]		84.7 ± 3.1	428.3 ± 16.9	343.6 ± 17.2	49.3 ± 4.4	267.7 ± 12.6	111.32 ± 8.1

[a]Sediment surface area, determined by multipoint BET N_2 adsorption.
[b]Determined by HF-phenanthroline analysis; values represent the mean ± SD of duplicate determinations.
[c]Determined from difference between total HF-phenanthroline extractable Fe and HF-phenanthroline extractable Fe(II);error terms calculated by error propagation.
[d]Determined by Mossbauer spectroscopy (see Figure 3); error terms were determined by propagation of uncertainties in model fits to Mossbauer spectra.
[e]No surface area data available.

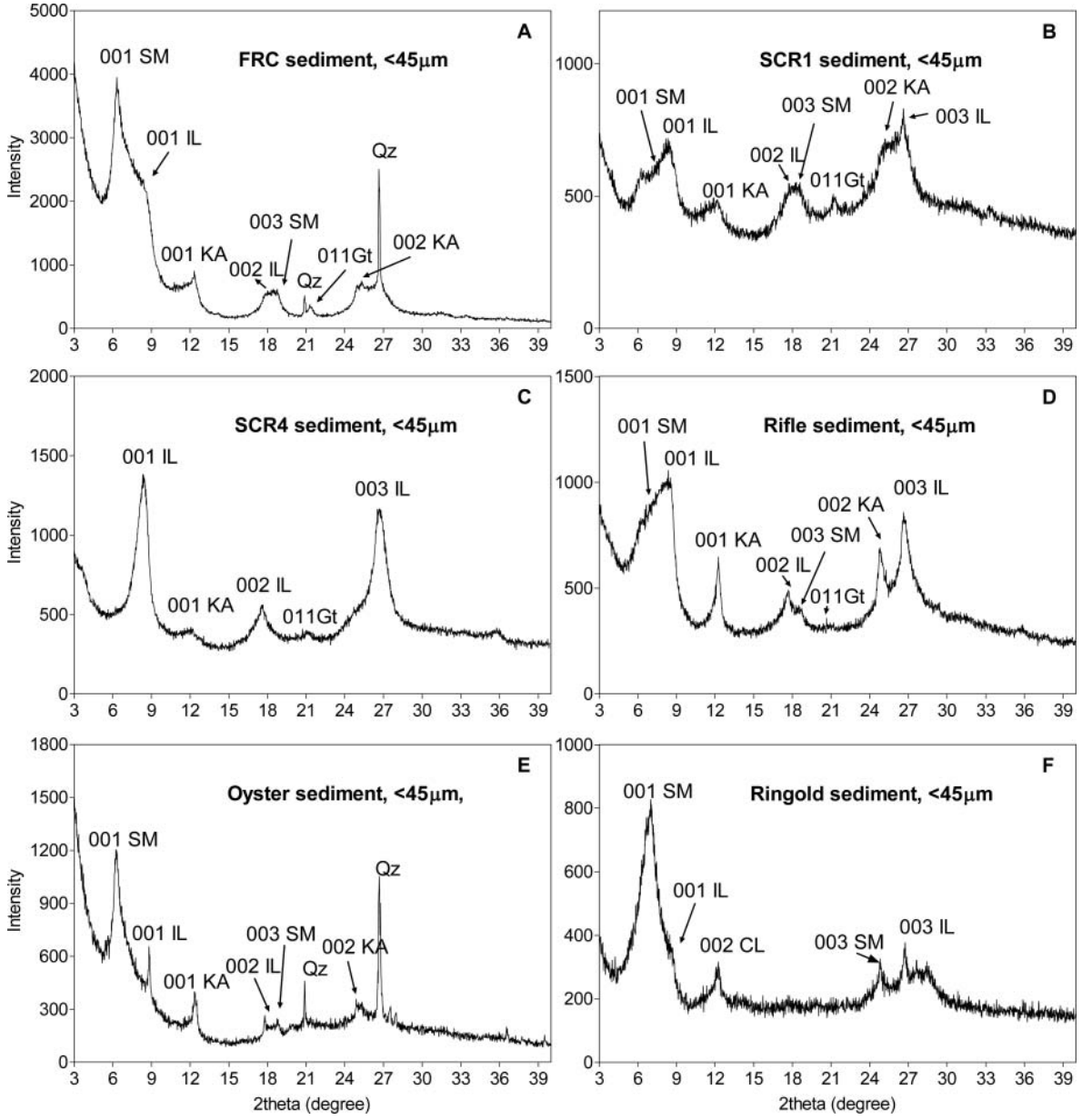

Figure 1. XRD patterns for the pristine subsurface sediments. SM is smectite; IL is illite; KA is kaolinite, Qz is quartz; Gt is goethite. The numbers associated with SM, IL and KA indicate the (hkl) planes in the minerals. The d-spacing values (Å) for the identified phases are as follows: 001 SM = 13.97; 001 IL = 10.54; 001 KA = 7.178; 004 IL = 4.962; 003 SM = 4.736; 002 KA = 3.562; 004 SM = 3.517.

phase in the FRC, Oyster and Ringold materials; in contrast, SCR1, SCR4 and Rifle contained relatively more illite. The smectite 001 peak ($2\Theta = 6.219°$; $d = 14.2$Å) and illite 001 peak ($2\Theta = 8.257°$; $d = 10.7$Å) were overlapped by broad peaks shown from 4° to 9° (2Θ) in the FRC, SCR1, Rifle and Ringold materials, which indicates the presence of mixed layer smectite-illite phases. Fe(III)-oxides (goethite) were detected by XRD only in the FRC materials.

Microbial reduction of pristine and CDB-extracted sediments

Each of the pristine and CDB-extracted/reoxidized materials underwent significant reduction by *G. sulfurreducens* (Figure 2). The total amount of Fe(II) produced was significantly higher for the pristine vs. the Fe(III) oxide stripped sediments, which can be attributed to partial reduction of Fe(III)-oxides in the pristine sediments. First-order rate constants for Fe(III) reduction ranged from ca. 0.008 to 0.2 d^{-1}, with no systematic trend among pristine vs. Fe(III) oxide stripped materials. The majority (93 ± 7%) of the Fe(II) produced during reduction of the pristine materials remained associated with the solid-phase, and there was no detectable release of Fe(II) to solution during microbial reduction of CDB-extracted materials. The culture medium for these experiments did not contain high concentrations of dissolved inorganic carbon or phosphate that could have facilitated formation of secondary Fe(II) minerals such as siderite or vivianite; hence, the near absence of aqueous Fe(II) production can be attributed to reassociation of biogenic Fe(II) with surface sites on clays and residual Fe(III)-oxides.

Low-temperature (12 K) Mossbauer spectroscopic analysis was used to determine the partitioning of solid-phase Fe during

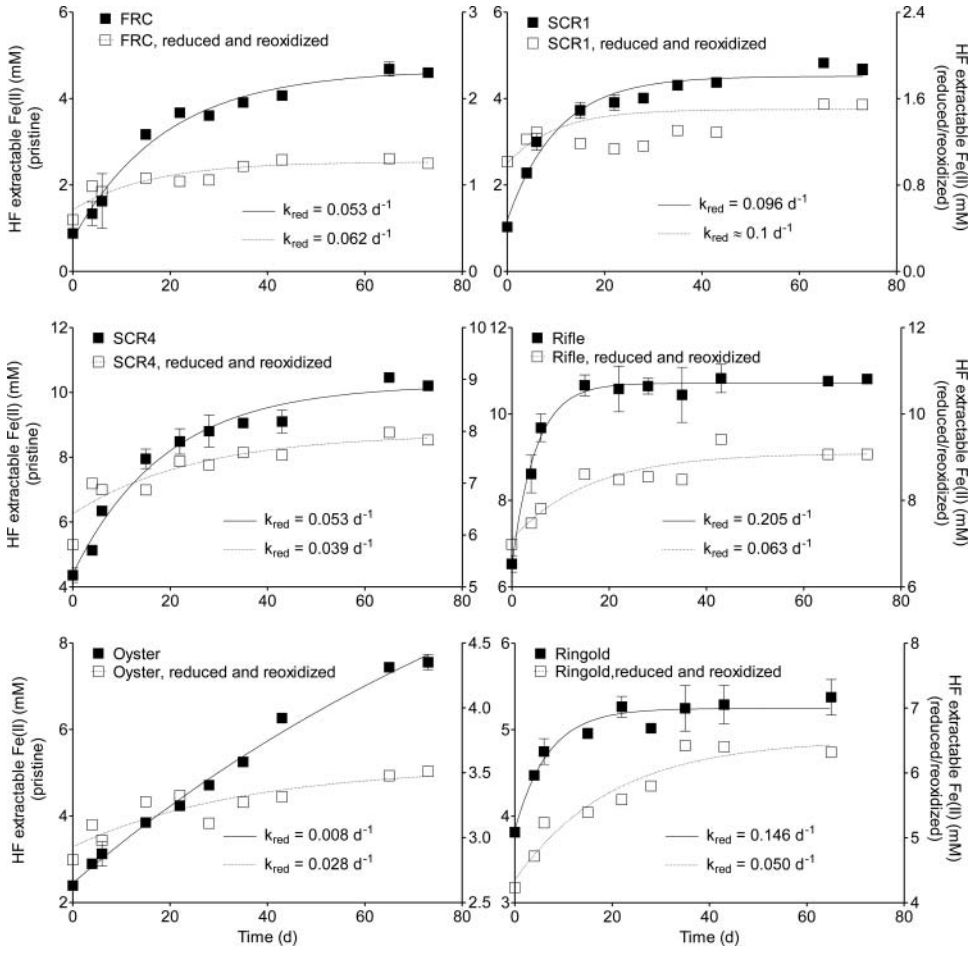

Figure 2. Microbial reduction of pristine and CDB-extracted/reoxidized subsurface sediments. Data represent the mean range of duplicate cultures. Solid and dashed lines show nonlinear least-squares regression fits of the data to an equation depicting the production of Fe(II) from a pool of microbially-reducible Fe(III) according to a first-order rate law: $Fe(II)_t = Fe(II)_0 + (Fe(II)_{max} - Fe(II)_0)\ [1 - exp(-k_{red}t)]$, where $Fe(II)_t$ is the Fe(II) concentration at time t, is the Fe(II) concentration at t = 0, $Fe(II)_{max}$ is the maximum concentration of Fe(II), and kred is the first-order reduction rate constant. $Fe(II)_0$, $Fe(II)_{max}$, and kred were each allowed to vary during the fitting procedure.

reduction of the pristine sediments (Figure 3). With the exception of the Ringold sediment, all of pristine materials showed a similar pattern (Figure 4) of a decrease in oxide-associated Fe, an increase in phyllosilicate-associated Fe(II), and only a small or insignificant change in phyllosilicate-associated Fe(III). For Ringold sediment (Figure 4f), the decrease in oxide-associated Fe was much less than other materials, likely due to the relatively low Fe(III) oxide content of the material.

Discussion

Fe partitioning during microbial Fe(III) reduction

The purpose of this research was to assess the interaction between microbial Fe(III) oxide and Fe(III) phyllosilicate reduction in relation to the relative abundance of the two phases in natural subsurface materials. The study was designed to complement an analogous examination of microbial reduction of Fe(III) oxide stripped, synthetic goethite-coated FRC sediment, i.e., one of the same materials included in this work (Wu et al. 2015). A previously developed model for Fe partitioning (Figure 10 in Wu et al. 2015) during microbial Fe(III) reduction was applied to interpretation of the data from this study. The model revolves around three possible pathways for partitioning of Fe(II) generated during microbial Fe(III) oxide reduction: (1) Fe(II) sorption to Fe(III)-oxides (f_1) which produces no change in oxide-Fe signal; (2) Fe(II) sorption to phyllosilicates (f_2), which produces an increase in phyllosilicate-Fe (II) signal; or (3) electron transfer from oxide-derived Fe(II) to Fe(III) phyllosilicate surfaces (f_3), which produces a decrease in phyllosilicate-Fe(III) signal and a parallel increase in oxide-Fe and phyllosilicate-Fe(II) signals. An additional factor, $f4$, corresponds to the fraction of total solid-phase Fe(II) production associated with Fe(III) oxide reduction. As explained in Wu et al. (2015), an inverse modeling approach was employed to obtain estimates for f_1, f_2, f_3 and f_4. The total amount of solid-phase Fe(II) produced at the end of the microbial reduction experiments [equal to total HF-phenanthroline extractable Fe (II) minus aqueous Fe(II)] was used to constrain the total change in Mossbauer signal across the three pools, and the Solver routine in Microsoft Excel was used to compute values for f_1, f_2, f_3 and f_4 that minimize the sum of the square of the differences between observed and calculated changes in oxide-Fe, phyllosilicate-Fe(II), and phyllosilicate-Fe(III) pool sizes. The percent of total Fe pool size change accounted for by the model predictions was computed by a sum of squared errors approach analogous to that employed in regression analysis (see Wu et al. 2015, for details).

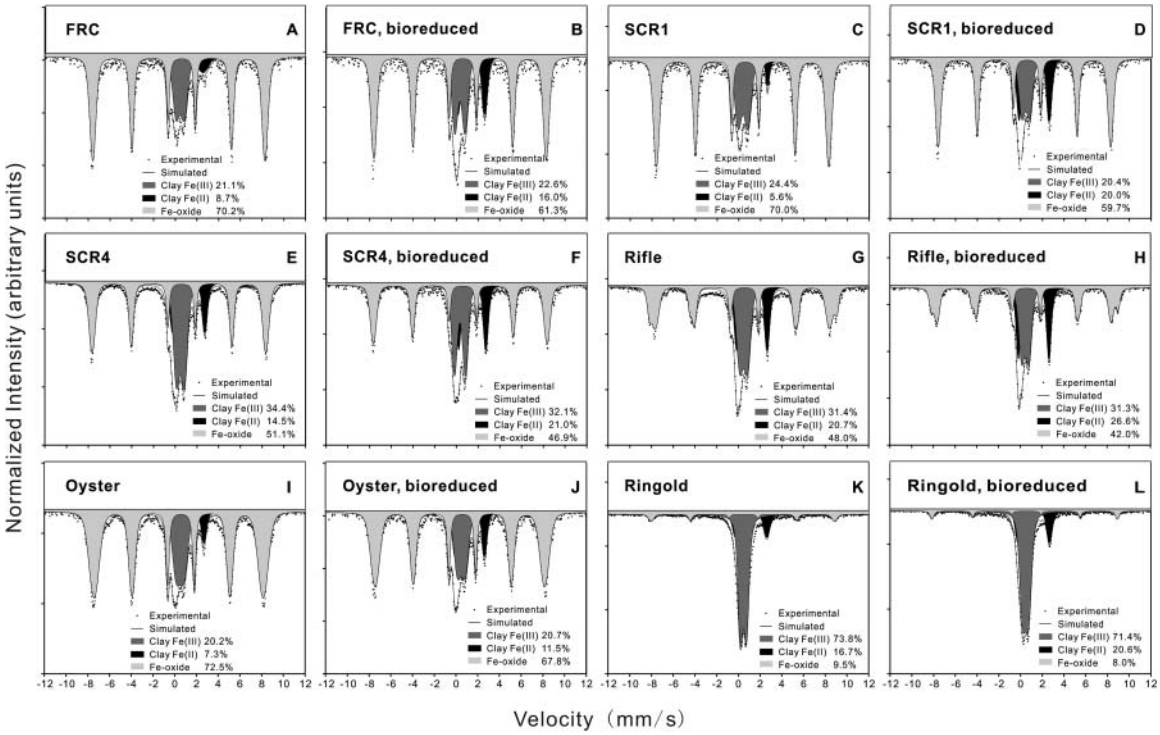

Figure 3. Mossbauer spectra for pristine subsurface sediments before and after microbial reduction.

The Fe partitioning model is based on assumptions derived from experimental observations. The first assumption, i.e., that Fe(II) sorbed to Fe(III) oxide surfaces produces no change in Mossbauer signal for oxide-Fe, is based on the finding that the Mossbauer spectra for microbially reduced pure synthetic goethite was identical to that for the unreduced mineral (Figure 5 in Wu et al. 2015). This finding is consistent with previous experiments with synthetic goethite, where sorption of ^{57}Fe-enriched Fe(II) to ^{56}Fe-goethite produced a ^{57}Fe signal in the goethite sextet in Mossbauer spectra (Williams and Scherer 2004). The second key assumption is that Fe(II) sorbed to phyllosilicate surfaces produces an increase the Mossbauer signal for phyllosilicate-Fe(II). This phenomenon has been observed in several studies (Dong et al. 2003; Kukkadapu et al. 2001, 2006) and results from the fact that Fe(II) associated with clay surface sites produces a doublet which overlaps the doublet for phyllosilicate-Fe(II) (Diamant et al. 1982). The final assumption is that Fe(II) derived from microbial Fe(III) oxide reduction has the potential to engage in electron transfer to Fe(III) phyllosilicate surfaces. This is a recently recognized phenomenon (Neumann et al. 2013; Schaefer et al. 2011), which was observed during abiotic Fe(II) sorption experiments reported in Wu et al. (2015).

With the exception of the Ringold sediment, the Fe partitioning model results (Table 2) indicate that Fe(III) oxide reduction dominated overall Fe(III) reduction activity ($f_4 \approx 1$).

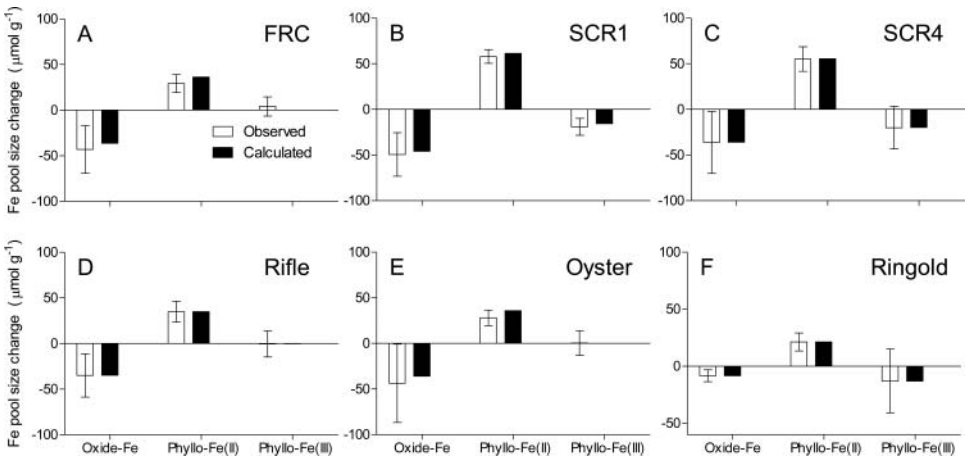

Figure 4. Mossbauer-derived changes in Fe pool sizes during microbial reduction of (a) FRC, (b) SCR1, (c) SCR4, (d) Rifle, (e) Oyster, and (f) Ringold sediment. Open bars show observed data; filled bars show results of Fe partitioning model calculations (see Discussion). Error terms for observed data were determined by propagation of uncertainties in model fits to Mossbauer spectra.

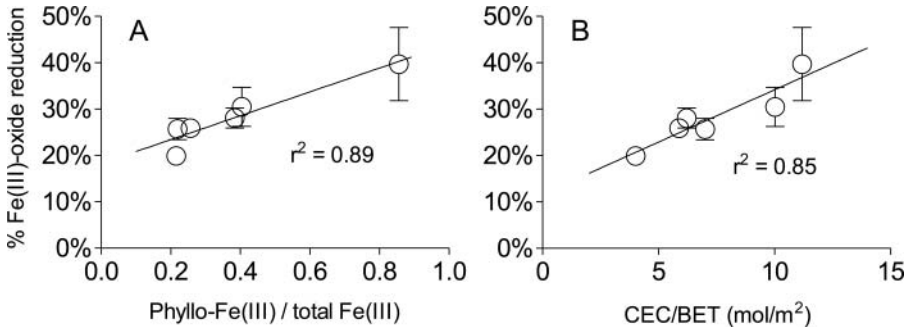

Figure 5. Correlation between the extent of Fe(III)-oxide reduction (see Table 3) and the ratio of Fe(III)-phyllo to total Fe(III) content (A) and surface area-normalized CEC (B). Lines show the results of linear least-squares regression analysis.

These results are directly analogous to those reported for the synthetic goethite-coated FRC sediment employed in Wu et al. (2015). It is notable that, in contrast to prior studies with specimen Fe(III)-phyllosilicates [see Dong et al. (2009) for review], variations in phyllosilicate mineralogy among the five Fe(III) oxide rich sediments (Figure 1) had essentially no impact on Fe (III) phyllosilicate reduction in the pristine sediment. Likewise, there was no obvious connection between phyllosilicate mineralogy and Fe(III) phyllosilicate reduction rate constants (see Figure 2) and extents of reduction for the Fe(III) oxide stripped sediments, which averaged 13.3 ± 6.1% and 0.057 ± 0.025 d^{-1}, respectively, across the FRC, SCR1, SCR4, Rifle and Oyster materials. The observed extents of reduction are comparable to those documented for specimen smectites in the absence of exogenous electron shuttling compounds such as AQDS, which are known to significantly increase the extent of Fe(III) phyllosilicate reduction (Jaisi et al. 2005, 2007b; Kostka et al. 1999; Seabaugh et al. 2006).

Fe(III) phyllosilicate reduction contributed significantly (ca. 33%) to total Fe(III) reduction in the pristine Ringold sediment. This result may be attributed to the relatively high Fe(III) phyllosilicate content of the Ringold material compared to the other five sediments (see Table 1). Nevertheless, it is striking that Fe (III) oxide reduction still dominated overall reduction activity despite the comparatively low Fe(III) oxide content of the material. Across all the materials, the Fe partitioning model results indicated that only 0–5% of the Fe(III) phyllosilicate content of the pristine materials was microbially reduced, compared to 7–17% for the Fe(III) oxide stripped materials. As discussed in Wu et al. (2015), the most straightforward way to interpret these results is that *G. sulfurreducens* preferentially attacked Fe(III) oxide coatings as opposed to Fe(III) centers on phyllosilicate surfaces. Whether or not this can be attributed to kinetic or thermodynamic factors is currently unknown. However, the specific surface area of the Fe(III) oxide coatings is likely to be significantly higher than the μm-sized clay particles, such that kinetic control posed by the availability of Fe(III) surface sites could have played a significant role in controlling oxide vs. phyllosilicate reduction. In addition, sorption of Fe (II) produced during Fe(III) oxide reduction to phyllosilicate surfaces (evidenced by f_2 values of 0.27–0.76 in Table 2), may have inhibited enzymatic electron transfer to Fe(III) phyllosilicate surfaces (Jaisi et al. 2007a, b).

The Fe partitioning model results suggest that there was only limited electron transfer from oxide-derived Fe(II) to Fe (III)-phyllosilicates (f_3 values $\leq$ 0.2 in Table 2). Here again, these results are consistent with those from microbial reduction experiments with synthetic goethite-coated FRC sediment (Wu et al. 2015), and different from abiotic Fe(II) sorption experiments with the same FRC material as well as synthetic Fe(III) phyllosilicate phases (Neumann et al. 2013; Schaefer et al. 2011). As previously discussed (Wu et al. 2015), the simplest explanation for these results is that rapid exposure of Fe(III) phyllosilicate surfaces to a large quantity of aqueous Fe(II) during sorption experiments leads to significant abiotic reduction, whereas Fe(II) accumulating more slowly during microbial reduction experiments becomes associated with oxide and phyllosilicate surface sites (i.e., cation exchange sites in the case of the clays) before electron transfer can take place.

Implications for previous studies

The finding that Fe(III) oxide reduction dominated overall Fe (III) reduction activity in the current experiments has important implications for interpreting previous and ongoing studies of Fe(III) oxide and Fe(III) phyllosilicate reduction in natural soils and sediments. In previous studies, the change in Mossbauer Fe(III) oxide signal compared to Fe(III) phyllosilicate signal has been used to directly infer the relative amount of oxide vs. phyllosilicate reduction (Kukkadapu et al. 2006; Komlos et al. 2007, 2008; Mohanty et al. 2008). This approach does not take

Table 2. Model-inferred Fe(II) partitioning during the microbial reduction experiments.

Material	f_1[a]	f_2[b]	f_3[c]	f_4[d]	% Variation explained[e]
FRC	0.73	0.27	0.0	1.0	94
SCR1	0.06	0.76	0.2	0.93	98
SCR4	0.55	0.30	0.1	0.98	100
Rifle	0.59	0.41	0.0	1.0	100
Oyster	0.59	0.41	0.0	1.0	90
Ringold	0.46	0.41	0.1	0.67	100

[a]Fraction of solid-associated Fe(II) that sorbed to Fe(III) oxides, as inferred from Fe partitioning model [Figure 10 in Wu et al. (2015)] calculations (see Discussion).
[b]Fraction of solid-associated Fe(II) that sorbed to Fe-phyllosilicates, producing a Fe (II) phyllosilicate signal, as inferred from Fe partitioning model calculations.
[c]Fraction of solid-associated Fe(II) that engaged in electron transfer to Fe(III) phyllosilicates, as inferred from Fe partitioning model calculations.
[d]Fraction of bulk Fe(III) reduction attributable to Fe(III) oxide reduction, as inferred from Fe partitioning model calculations.
[e]Percent of total variation among observed pool size changes accounted for by Fe partitioning model calculations [see Discussion section in Wu et al. (2015)].

Table 3. Fractional contribution of Fe(III) oxide reduction to total Fe(III) reduction determined directly from Mossbauer spectral data, compared to that estimated from the Fe partitioning model.

Study	Sediment	Direct calculation	Fe partitioning model	Ratio[a]
Wu et al. (2012)	Pristine FRC	0.60	0.80	1.34
Wu et al. (2015)	Fe(III) oxide stripped, synthetic goethite-coated FRC	0.77	0.98	1.27
This study	SRC1	0.72	0.93	1.29
This study	SRC4	0.64	0.98	1.52
This study	Rifle	0.99	1.0	1.01
This study	Ringold	0.39	0.67	1.70
Kukkadapu et al. (2006)	FRC	0.45	1.0	2.2
Komlos et al. (2007)	Rifle	0.13	1.0	8.0
Komlos et al. (2008)	Rifle	0.53	1.0	1.9
Mohanty et al. (2008)	SCR1	0.74	0.99	1.3

[a]Ratio of Fe partitioning model result to direct calculation.

Table 4. Inferred Fe(II) partitioning in previously published Mossbauer-based studies of sediment Fe(III) oxide and Fe(III) phyllo reduction.

Study	Material/DIRB	f_1[a]	f_2[b]	f_3[c]	f_4[d]	% Variation explained[e]
Kukkadapu et al. (2006)	FRC + *S. putrefaciens*	0.47	0.53	0.0	1.0	100
Komlos et al. (2007)	Rifle + sediment microbes	0.18	0.19	0.63	1.0	100
Komlos et al. (2008)	Rifle + sediment microbes	0.21	0.60	0.19	0.99	75
Mohanty et al. (2008)	SCR1 + sediment microbes	0.0	0.76	0.24	1.0	100

[a]Fraction of solid-associated Fe(II) that sorbed to Fe(III) oxides, as inferred from Fe partitioning model [Figure 10 in Wu et al. (2015)] calculations (see Discussion).
[b]Fraction of solid-associated Fe(II) that sorbed to Fe-phyllosilicates, producing a Fe(II) phyllosilicate signal, as inferred from Fe partitioning model calculations.
[c]Fraction of solid-associated Fe(II) that engaged in electron transfer to Fe(III) phyllosilicates, as inferred from Fe partitioning model calculations.
[d]Fraction of bulk Fe(III) reduction attributable to Fe(III) oxide reduction, as inferred from Fe partitioning model calculations.
[e]Percent of total variation among observed pool size changes accounted for by Fe partitioning model calculations [see Discussion section in Wu et al. (2015)].

into account the fact that Fe(II) sorbed to residual Fe(III) oxide surfaces contributes to the Mossbauer signal for Fe(III) oxide, thus biasing downward Mossbauer-derived estimates of Fe(III) oxide reduction. Inherent uncertainties in changes in Fe(III) phase abundances inferred from fitting of Mossbauer spectra complicates making a comprehensive analysis of the quantitative significance of this phenomenon across all the experimental data reported here and in Wu et al. (2012, 2015): in four out of ten experiments with pristine or synthetic goethite-coated sediments [two in Wu et al. (2015) and two in this study], there was either no change or a small increase in the Mossbauer Fe (III) phyllosilicate signal, which prevents making a direct calculation of Fe(III) oxide vs. Fe(III) phyllosilicate reduction. However, this was possible for the other six experiments, and the results indicate that direct calculation of Fe(III) oxide reduction from Mossbauer data underestimated oxide reduction by a factor of up to 1.7 compared to Fe partitioning model calculations (see Table 3). Application of the Fe partitioning model to data from four previously published studies of subsurface sediment microbial Fe(III) reduction (Kukkadapu et al. 2006; Komlos et al. 2007, 2008; Mohanty et al. 2008) (Figure 5) indicate that direct calculation of Fe(III) oxide and Fe(III) phyllosilicate reduction from Mossbauer accounted for virtually all Fe(III) reduction (Table 4) and underestimated oxide reduction by a factor of 1.8–8 (Table 3). These results emphasize that future Mossbauer studies of Fe(III) oxide and Fe(III) phyllosilicate reduction in natural sediments need to take this effect into account, e.g., through application of the Fe partitioning model.

Controls on the extent of Fe(III) oxide reduction

Although the results from this study showed little or no enzymatic Fe(III) phyllosilicate reduction except for the phyllosilicate-rich Ringold material, this does not mean the presence of phyllosilicates does not influence overall Fe(III) reduction activity. Phyllosilicates have the potential to sorb biogenic Fe (II) derived from Fe(III) oxide reduction, and thereby enhance Fe(III) oxide reduction by reducing or delaying the inhibitory effect that Fe(II) accumulation on oxide and DIRB cell surfaces has on oxide reduction (Urrutia et al. 1999). This effect was

Table 5. Extent of microbial Fe(III) oxide reduction in pristine subsurface materials.

Sample	Fe(III) oxide reduction[a] (μ mol/g)	% Fe(III) oxide reduction	Fe(III) Phyllo/Total Fe(III)[b]	CEC[c] (mol/m^2)
FRC	76.1 ± 4.6	25.7 ± 2.3	0.22 ± 0.02	7.0
SCR1	75.9 ± 3.3	25.9 ± 2.0	0.26 ± 0.02	5.9
SCR4	122.0 ± 6.3	28.1 ± 2.2	0.38 ± 0.03	6.2
Rifle	85.8 ± 10.7	30.5 ± 4.2	0.40 ± 0.03	10.0
Oyster	103.3 ± 5.0	19.9 ± 1.5	0.22 ± 0.02	4.0
Ringold	20.9 ± 3.9	35.6 ± 7.1	0.86 ± 0.06	11.2

[a]Determined from total HF-phenanthroline extractable Fe(II) production and the factor f_4 in Table 2.
[b]Ratio of Fe(III) phyllo to total Fe(III) content (data from Table 1).
[c]Surface area-normalized cation exchange capacity (CEC).

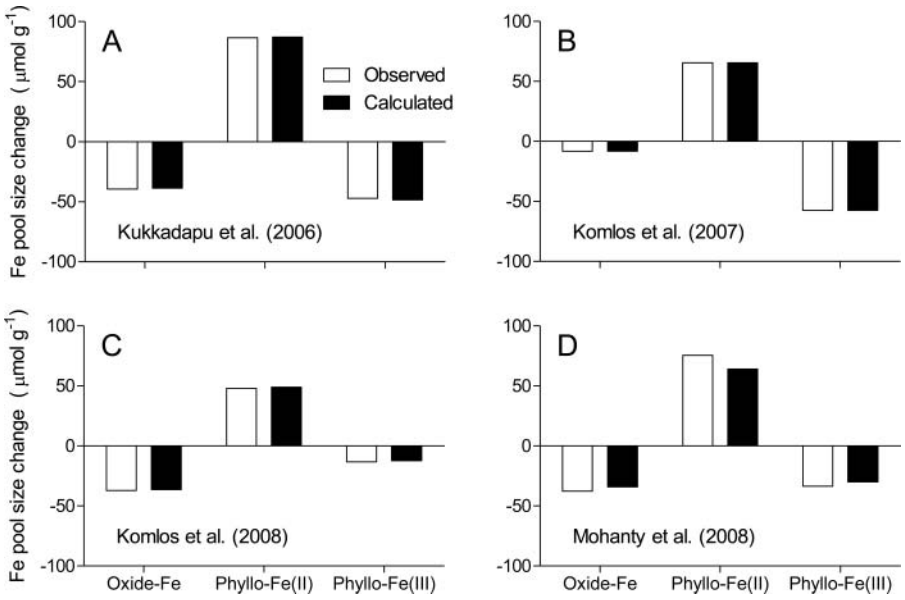

Figure 6. Mossbauer-derived changes in Fe pool sizes during previously-published subsurface sediment microbial reduction experiments. Open bars show observed data; filled bars show results of Fe partitioning model calculations (see Discussion).

observed in Wu et al. (2015), where reduction of synthetic goethite coated onto Fe(III) oxide stripped FRC sediment was 1.5- to 2-fold greater than reduction of the pure oxide. Although it is not possible to make such direct comparisons for natural sediments [because of difficulties in physically separating oxides and phyllosilicates in sediments; Wu et al. (2012)], we did observe a strong positive correlation between the extent of Fe(III) oxide reduction (inferred from Fe partitioning model calculations; Table 5) and (1) the relative abundance of Fe(III) phyllosilicate to bulk total sediment Fe(III) (see Figure 5a), as well (2) the surface area-normalized cation (NH_4^+) exchange capacity (CEC) of the different sediments (Figure 5b). bib18-Phyllosilicates, especially smectites, have much higher CEC than other soil and sediment minerals, including Fe(III)-oxides (Yuan and Theng 2011). Hence, surface area-normalized CEC was likely indicative of the Fe(II)-binding capacity of the native phyllosilicates. The correlation between the extent of oxide reduction and the relative abundance and CEC of sediment phyllosilicates is consistent with the idea that binding of oxide-derived Fe(II) by phyllosilicates can promote Fe(III) oxide reduction. These findings provide empirical support for reaction models of sediment Fe(III) oxide reduction that take into account the influence of Fe(II) sorption onto "auxiliary" mineral surfaces as a key control on long-term oxide reduction kinetics (Jin and Roden 2011; Roden 2008).

Conclusion

This study together with the companion paper (Wu et al. 2015) expands our knowledge of the interaction between Fe(III)-oxides and Fe(III)-phyllosilicates during microbial reduction in subsurface sediments. In particular, this work is the first to address all of the major Fe partitioning phenomena that may influence the relative extent of Fe(III) oxide vs. Fe(III) phyllosilicate reduction. The results suggest that Fe(III) oxide reduction is typically underestimated when changes in Mossbauer-derived Fe(III) oxide abundance are used directly to estimate Fe(III) oxide reduction, because oxide-derived biogenic Fe(II) that reassociates with Fe(III) oxide surfaces contributes to the Mossbauer Fe(III) oxide signal. Application of a Fe partitioning model that takes this effect into account led to the conclusion that Fe(III) oxide reduction dominated overall Fe(III) reduction in each of the sediments examined here; even in materials (Ringold formation) that had a very high abundance of Fe(III)-phyllosilicates (i.e., compared to Fe(III)-oxides), Fe(III) oxide reduction accounted for ca. two-thirds of overall reduction activity. Nevertheless, our data indicate that the presence of phyllosilicates can significantly influence overall Fe(III) reduction activity by binding oxide-derived Fe(II), thereby counteracting the passivating effect that accumulation of Fe(II) on oxide and DIRB surfaces has on Fe(III) oxide reduction. Although our results indicate that electron transfer from oxide-derived Fe(II) to Fe(III) phyllosilicate surfaces did not have a major impact on Fe partitioning during microbial reduction, this as well as the aforementioned phenomena should be carefully considered in all future studies of Fe(III) reduction in subsurface sediments that contain significant quantities of both Fe(III)-oxides and Fe(III)-phyllosilicates.

Funding

This research was funded by the U.S. DOE, Office of Biological and Environmental Research, through grants DE-FG02-06ER64184 and ER64172-1027487-001191 from the Environmental Remediation Science Program, grant DE-SC0001180 from the Subsurface Biogeochemical Research Program, and the SBR Scientific Focus Area at the Pacific Northwest National Laboratory.

References

Akob DM, Mills HJ, Gihring TM, Kerkhof L, Stucki JW,Anastacio AS, et al. 2008. Functional diversity and electron donor dependence of

microbial populations capable of U(VI) reduction in radionuclide-contaminated subsurface sediments. Appl Environ Microbiol 74:3159–3170.

Amonette JE, Templeton JC. 1998. Improvements to the quantitative assay of nonrefractory minerals for Fe(II) and total Fe using 1,10-phenanthroline. Clay Clay Min 46:51–62.

Anderson RT, Vrionis HA, Ortiz-Bernad I, Resch CT,Long PE, Dayvault R, et al. 2003. Stimulating the in situ activity of Geobacter species to remove uranium from the groundwater of a uranium-contaminated aquifer. Appl Environ Microbiol 69:5884–5891.

Barnett MO, Jardine PM, Brooks SC, Selim HM. 2000. Adsorption and transport of uranium(VI) in subsurface media. Soil Sci Soc Am J 64:908–917.

Bevington PR, Robinson DK. 1992. Data reduction and error analysis for the physical sciences. New York: McGraw Hill.

Bishop ME, Dong HL, Kukkadapu RK, Liu CX, Edelmann RE. 2011. Bioreduction of Fe-bearing clay minerals and their reactivity toward pertechnetate (Tc-99). Geochim Cosmochim Acta 75:5229–5246.

Caccavo F, Lonergan DJ, Lovley DR, Davis M, Stolz JF, McInerney MJ. 1994. *Geobacter sulfurreducens* sp. nov., a hydrogen- and acetate-oxidizing dissimilatory metal-reducing microorganism. Appl Environ Microbiol 60:3752–3759.

Diamant A, Pasternak M, Banin A. 1982. Characterization of adsorbed iron in montmorillonite by Mossbauer spectroscopy. Clays Clay Min 30:63–66.

Dong HL, Jaisi DP, Kim J, Zhang GX. 2009. Microbe-clay mineral interactions. Am Miner 94:1505–1519.

Dong HL, Kukkadapu RK, Fredrickson JK, Zachara JM, Kennedy DW, Kostandarithes HM. 2003. Microbial reduction of structural Fe(III) in illite and goethite. Environ Sci Technol 37:1268–1276.

Fredrickson JK, Kota S, Kukkadapu RK, Liu CX, Zachara JM. 2003. Influence of electron donor/acceptor concentrations on hydrous ferric oxide (HFO) bioreduction. Biodegradation 14:91–103.

Fredrickson JK, Zachara JM, Kennedy DW, Dong HL, Onstott TC, Hinman NW, Li SM. 1998. Biogenic iron mineralization accompanying the dissimilatory reduction of hydrous ferric oxide by a groundwater bacterium. Geochim Cosmochim Acta 62:3239–3257.

Jaisi DP, Dong H, Liu C. 2007a. Kinetic analysis of microbial reduction of Fe(III) in nontronite. Environ Sci Technol 41:2437–2444.

Jaisi DP, Dong HL, Liu CX. 2007b. Influence of biogenic Fe(II) on the extent of microbial reduction of Fe(III) in clay minerals nontronite, illite, and chlorite. Geochim Cosmochim Acta 71:1145–1158.

Jaisi DP, Kukkadapu RK, Eberl DD, Dong HL. 2005. Control of Fe(III) site occupancy on the rate and extent of microbial reduction of Fe(III) in nontronite. Geochim Cosmochim Acta 69:5429–5440.

Jin Q, Roden EE. 2011. Microbial physiology-based model of ethanol metabolism in subsurface sediments. J Contam Hydrol 125:1–12.

Komadel P, Stucki JW. 1988. Quantitative assay of minerals for Fe^{2+} and Fe^{3+} using 1,10-Phenanthroline.3. A rapid photochemical method. Clay Clay Min 36:379–381.

Komlos J, Kukkadapu RK, Zachara JM, Jaffe PR. 2007. Biostimulation of iron reduction and subsequent oxidation of sediment containing Fe-silicates and Fe-oxides: effect of redox cycling on Fe(III) bioreduction. Water Res 41:2996–3004.

Komlos J, Peacock A, Kukkadapu RK, Jaffe PR. 2008. Long-term dynamics of uranium reduction/reoxidation under low sulfate conditions. Geochim Cosmochim Acta 72:3603–3615.

Kostka JE, Haefele E, Viehweger R, Stucki JW. 1999. Respiration and dissolution of iron(III) containing clay minerals by bacteria. Environ Sci Technol 33:3127–3133.

Kukkadapu RK, Zachara JM, Fredrickson JK, Kennedy DW. 2004. Biotransformation of two-line silica-ferrihydrite by a dissimilatory Fe(III)-reducing bacterium: formation of carbonate green rust in the presence of phosphate. Geochim Cosmochim Acta 68:2799–2814.

Kukkadapu RK, Zachara JM, Fredrickson JK, McKinley JP, Kennedy DW, Smith SC, Dong HL. 2006. Reductive biotransformation of Fe in shale-limestone saprolite containing Fe(III)-oxides and Fe(II)/Fe(III)-phyllosilicates. Geochim Cosmochim Acta 70:3662–3676.

Kukkadapu RK, Zachara JM, Smith SC, Fredrickson JK, Liu C. 2001. Dissimilatory bacterial reduction of Al-substituted goethite in subsurface sediments. Geochim Cosmochim Acta 65:2913–2924.

Lee JH, Fredrickson JK, Kukkadapu RK, Boyanov MI, Kemner KM, Lin XJ, et al. 2012. Microbial reductive transformation of phyllosilicate Fe(III) and U(VI) in fluvial subsurface sediments. Environ Sci Technol 46:3721–3730.

Liu D, Dong H, Bishop ME, Zhang J, Wang H, Xie S, et al. 2012. Microbial reduction of structural iron in interstratified illite-smectite minerals by a sulfate-reducing bacterium. Geobiology 10:150–162.

Lovley DR. 1993. Dissimilatory metal reduction. Annu Rev Microbiol 47:263–290.

Lovley DR, Phillips EJP. 1988. Novel mode of microbial energy metabolism: organic carbon oxidation coupled to dissimilatory reduction of iron or manganese. Appl Environ Microbiol 54:1472–1480.

Luan F, Gorski CA, Burgos WD. 2014. Thermodynamic controls on the microbial reduction of iron-bearing nontronite and uranium. Environ Sci Technol 48:2750–2758.

Luan FB, Gorski CA, Burgos WD. 2015a. Linear free energy relationships for the biotic and abiotic reduction of nitroaromatic compounds. Environ Sci Technol 49:3557–3565.

Luan FB, Liu Y, Griffin AM, Gorski CA, Burgos WD. 2015b. Iron(III)-bearing clay minerals enhance bioreduction of nitrobenzene by *Shewanella putrefaciens* CN32. Environ Sci Technol 49:1418–1426.

Mehra OP, Jackson ML. 1960. Iron oxide removal from soils and clays by a dithionite-citrate system buffered with sodium bicarbonate. clays and clay minerals. In: Proceedings of the 7th National Congress, Pergamon, London.

Methe BA, Nelson KE, Eisen JA, Paulsen IT, Nelson W, Heidelberg JF, et al. 2003. Genome of *Geobacter sulfurreducens*: metal reduction in subsurface environments. Science 302:1967–1969.

Mohanty SR, Kollah B, Hedrick DB, Peacock AD, Kukkadapu RK, and Roden EE. 2008. Biogeochemical processes in ethanol stimulated uranium-contaminated suhsurface sediments. Environ Sci Technol 42:4384–4390.

Moon JW, Roh Y, Phelps TJ, Phillips DH, Watson DB, Kim YJ, Brooks SC. 2006. Physicochemical and mineralogical characterization of soil-saprolite cores from a field research site, Tennessee. J Environ Qual 35:1731–1741.

Neumann A, Olson TL, Scherer MM. 2013. Spectroscopic evidence for Fe (II)-Fe(III) electron transfer at clay mineral edge and basal sites. Environ Sci Technol 47:6969–6977.

Penn RL, Zhu C, Xu H, Veblen DR. 2001. Iron oxide coatings on sand grains from the Atlantic coastal plain: high-resolution transmission electron microscopy characterization. Geology 29:843–846.

Pentrakova L, Su K, Pentrak M, Stuck JW. 2013. A review of microbial redox interactions with structural Fe in clay minerals. Clay Minerals 48:543–560.

Rancourt DG, Ping JY. 1991. Voigt-based methods for arbitrary-shape static hyperfine parameter distributions in Mossbauer-spectroscopy. Nucl Instrum Meth Phys Rev 58:85–97.

Roden EE. 2008. Microbiological controls on geochemical kinetics 1: fundamentals and case study on microbial Fe(III) reduction. In: Brantley SL, Kubicki J, and White AF, editors. Kinetics of Water-Rock Interactions. New York: Springer, p335–415.

Roden EE, Zachara JM. 1996. Microbial reduction of crystalline iron(III) oxides: influence of oxide surface area and potential for cell growth. Environ Sci Technol 30:1618–1628.

Sawhney BL. 1989. Interstratification in layer silicates. In: Dixon JB and Weed SB, editors. Minerals in Soil Environments, 2nd ed. Madison, WI: Soil Science Society of America, p789–828.

Schaefer MV, Gorski CA, Scherer MM. 2011. Spectroscopic evidence for interfacial Fe(II)-Fe(III) electron transfer in a clay mineral. Environ Sci Technol 45:540–545.

Seabaugh JL, Dong HL, Kukkadapu RK, Eberl DD, Morton JP, Kim J. 2006. Microbial reduction of Fe(III) in the Fithian and Muloorina illites: contrasting extents and rates of bioreduction. Clay Clay Min 54:67–79.

Stucki JW, Kostka JE. 2006. Microbial reduction of iron in smectite. C R Geosci 338:468–475.

Sumner ME, Miller WP. 1996. Cation exchange capacity and exchange coefficients. In: Bigham JM, editor. Methods of Soil Analysis, Part 3. Chemical Methods. Madison, WI: Soil Science Society of America, p1201–1230.

Urrutia MM, Roden EE, Zachara JM. 1999. Influence of aqueous and solid-phase Fe(II) complexants on microbial reduction of crystalline Fe(III)-oxides. Environ Sci Technol 33:4022–4028.

Williams AGB, Scherer MM. 2004. Spectroscopic evidence for Fe(II)-Fe (III) electron transfer at the iron oxide-water interface. Environ Sci Technol 38:4782–4790.

Wu T, Kukkadapu R, Griffin AM, Gorski CA, Konishi H, Xu H, Roden EE. 2015. Interactions between Fe(III)-oxides and Fe(III)-phyllosilicates during microbial reduction 1: synthetic sediments. Geomicrobiol J. In press.

Wu T, Shelobolina E, Xu H, Konishi H, Kukkadapu R, Roden EE. 2012. Isolation and microbial reduction of Fe(III)-phyllosilicates from subsurface sediments. Environ Sci Technol 46:11618−11626.

Yuan G, Theng BKG. 2011. Clay-organic interaction in soil environments. In: Huang ME, Li PM, and Sumner Y, editors. Handbook of Soil Sciences: Resource Management and Environmental Impacts, 2nd ed. Boca Raton, FL: CRC Press.

Zachara JM, Fredrickson JK, Li SW, Kennedy DW, Smith SC, Gassman PL. 1998. Bacterial reduction of crystalline Fe(III)-oxides in single phase suspension and subsurface materials. Am Miner 83:1426–1443.

Zachara JM, Kukkadapu RK, Fredrickson JK, Gorby YA, Smith SC. 2002. Biomineralization of poorly crystalline Fe(III)-oxides by dissimilatory metal reducing bacteria (DMRB). Geomicrobiol J 19:179–207.

Zachara JM, Smith SC, Kuzel LS. 1995. Adsorption and dissociation of co-edta complexes in iron oxide-containing subsurface sands. Geochim Cosmochim Acta 59:4825–4844.

Zhang J, Dong HL, Liu D, Fischer TB, Wang S, Huang LQ. 2012. Microbial reduction of Fe(III) in illite-smectite minerals by methanogen Methanosarcina mazei. Chem Geol 292:35–44.